Section 5

Development of and studies with regional and smaller-scale atmospheric models, regional ensemble, monthly and seasonal forecasting

Arome WMED, a model dedicated to the HyMeX campaign

Nadia Fourrié, Emilie Bresson, Eric Sevault and Mathieu Nuret
CNRM-GAME, Météo-France and CNRS, 42 av Coriolis, 31057 Toulouse, France
Nadia.Fourrie@meteo.fr

HyMeX (HYdrological cycle in the Mediterranean Experiment, http://www.hymex.org) aims at a better understanding and quantification of the hydrological cycle and related processes in the Mediterranean Sea, with an emphasis on high-impact weather events, inter-annual to decennial variability of the Mediterranean coupled system, and associated trends in the context of global change. The 2012-2013 first HyMeX Special Observation Period (SOP) series targeted on the north-western Mediterranean area. The SOP1, from 5 September to 6 November 2012, was dedicated to heavy precipitation and flash-flooding. The SOP2, February- mid-March 2013 aimed at studying intense air-sea exchanges and dense water formation. The choice of this period of the year also allowed to document the Mediterranean cyclogenesis. A special AROME version, called AROMEWMED, was developed at CNRM to provide real time forecasts to the HyMeX operational centre and for the decision making of the observation deployment.

AROMEWMED is a HyMeX-dedicated version of the French operational AROME system (Seity et al, 2011) covering a domain which encompass Portugal to Italy, North Africa to France (34N -9W/ 48N-20E, see Figure 1). Its domain is 11% bigger than the operational one and is defined by 960 by 640 points. Sea surface represents 47% of the domain against 41% for the AROME model. The lateral boundary conditions are provided by the French global model ARPEGE every each hour. A 48 hour forecast was established once a day at 000TC. A 3-hour assimilation cycle is run with a three dimensional variational data assimilation system at an horizontal resolution of 2.5 km. A background error covariance matrix specific to AROMEWMED has been computed, using the ensemble approach proposed by Brousseau et al. (2012), over a 3 week-period during Autumn 2010 characterized by several active convective periods over the Mediterranean zone.

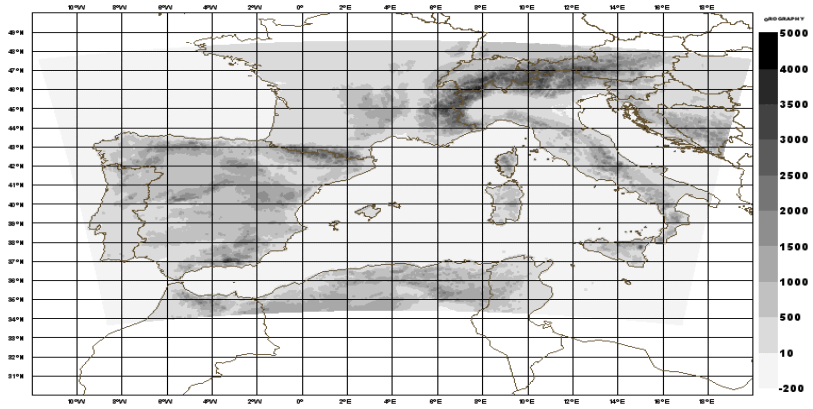

Figure 1: Orography (m) and domain of the AROMEWMED model.

The assimilated observations are the same as the ones used in the operational AROME model: radiosondes, surface data, wind profilers, ship and buoy report, aircraft reports, automated land surface stations. Satellites data are also assimilated: radiances from SEVIRI (Spinning Enhanced Visible and Infrared Imager) and from polar orbiting satellites, winds from atmospheric motion vectors (AMVs) and from scatterometers and GPS Zenith Tropospheric Delay (GPS-ZTD) observations. French network Radar data are also assimilated as Doppler wind (Montmerle and Faccani, 2009) and reflectivities provide information on relative humidity (Caumont et al, 2010, Wattrelot et al, 2008). Despite real time constraints, more satellite micro-wave observations and additional Spanish surface data were used in the analyses to improve the data coverage. A few observations of the field

campaign (Boundary layer pressurized balloons, additional radiosondes) have been also assimilated.

Figure 2 gives an example of the 24 hours rainfall rate predicted at 48- and 24- hour ranges with AROMEWMED for the 26 October 2012 and the rainfall rate observed with raingauges. This case corresponds to a Cevenol event and to high precipitations in Liguria-Tuscany and in central Italy, followed by flash floods. Theses precipitating events are forecasted by the model at a one day- and two day- ranges. In addition, a special effort was made to increase the verification data density with additional Spanish and Italian surface data, provided from meteorological centres in near real-time.

These mesoscale meteorological fields are available in the HyMeX database (http://mistrals.sedoo.fr/HyMeX/) and a first reanalysis, which takes into account a maximum of available observations, is under way.

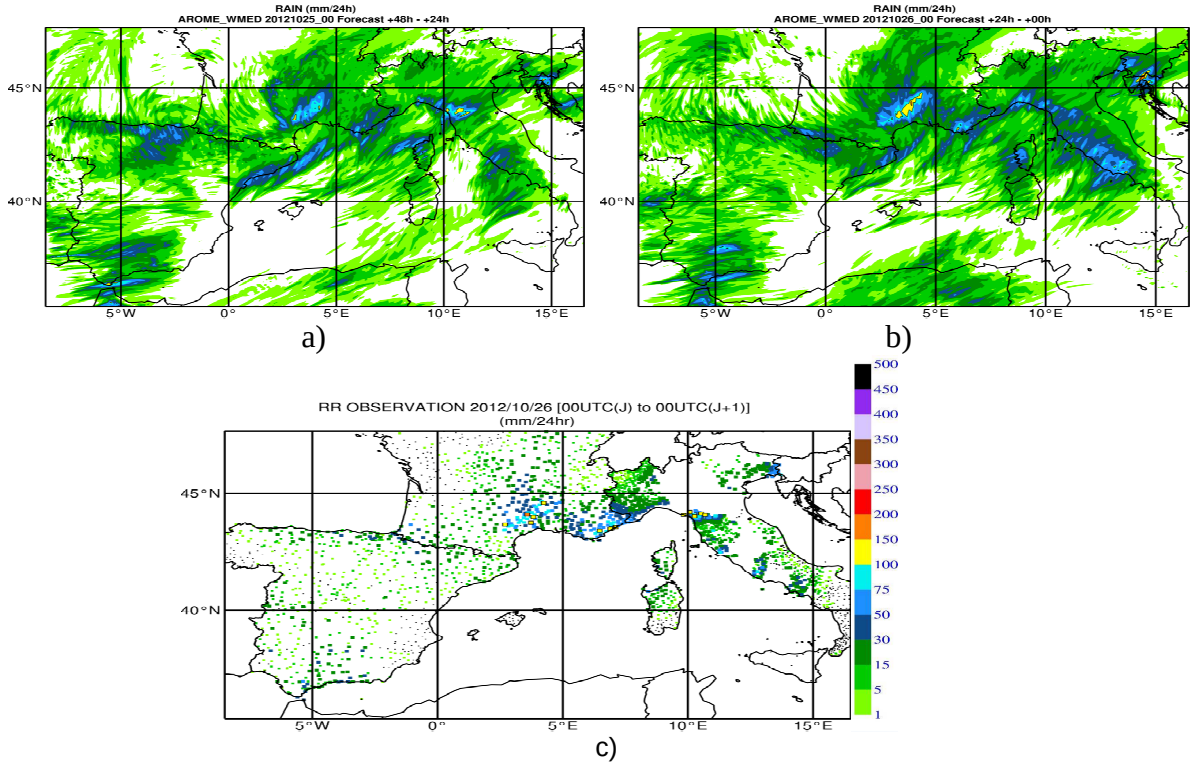

Figure 2: 24-hour rain rate (mm) predicted by the AROMEWMED model at the 48-hour range from the 25 October 2012 (a), at the 24-hour range from the 26 October 2012 (b) and 24-hour rainfall rate observed the 26 October 2012 with raingauges(c).

References:

Brousseau, P., L. Berre, F. Bouttier, and G. Desroziers, 2012: Background error covariances for a convective-sacle data-assimilation system : AROME-France 3D-Var. Quart. J. R. Meteorol. Soc., 137, 409–422.

Caumont, O., V. Ducrocq, E. Wattrelot, G. Jaubert, and S. Pradier-Vabre, 2010: 1D+3DVar assimilation of radar reflectivity data: A proof of concept. Tellus, 62, 173–187.

Michel, Y., T. Auligné T., and T. Montmerle, 2011: Heterogeneous convective-scale Background Error Covariances with the inclusion of hydrometeor variables. Mon.Wea.Rev., 139, 2994–3015.

Montmerle, T. and C. Faccani, 2009: Mesoscale assimilation of radial velocities from Doppler radars in a preoperational framework. Mon.Wea.Rev., 137, 1939–1953.

Seity, Y., P. Brousseau, S. Malardel, H. Hello, P. Bénard, F. Bouttier, C. Lac, and V. Masson, 2011: The AROME-France convective scale operational model. Mon.Wea.Rev., 139, 976–991.

Wattrelot, E., O. Caumont, S. Pradier-Vabre, M. Jurasek, and G. Haase, 2008: 1D+3DVar assimilation of radar reflectivities in the pre-operational AROME model at Météo-France. Fifth Conf on Radar in Meteorology and Hydrology, Helsinki, Finland. Finnish Meteorological Institute.,[Available online at http://erad2008.fmi.fi/prtoceedings/extended/erad2008–0097–extended.pdf].

The operational convection-permitting regional model at JMA

TABITO HARA, TADASHI FUJITA, SATOSHI MORIYASU, KOHEI KAWANO, YASUTAKA IKUTA,
YUTA HAYASHI, KENGO MATSUBAYASHI, NOBUMIKI KINOSHITA AND HISAKI EITO
Numerical Prediction Division, Japan Meteorological Agency
1-3-4, Ote-machi, Chiyoda-ku, Tokyo 100-8122, Japan

1 Introduction

In June 2012, the Japan Meteorological Agency (JMA) began operation of a new supercomputer system for numerical weather prediction (NWP). Leveraging its high performance specifications, a high resolution convection-permitting NWP system has been operated since August 2012 to provide information for aviation operation and disaster prevention. This report briefly introduces the design of the NWP system, which consists of analysis and forecast parts, and outlines some typical results.

2 Basic design of the Local NWP System

The high resolution operational NWP system (called "Local NWP system") currently covers the eastern part of Japan, and provides 9-hour forecasts every 3 hours. In the system design, high resolution to permit explicit convection and frequent updates of forecasts assimilating latest observation are highly emphasized. The NWP model (called the Local Forecast Model; LFM), which is one of two subsystems in the Local NWP system, has 2-km horizontal gridspacing and 60 vertical layers. Both of these specifications are superior to those of the Meso-Scale Model (MSM), which was the finest resolution model in JMA's operational NWP system before the Local NWP system was launched. Local Analysis (LA; the other subsystem) employs an analysis cycle based on three dimensional variational data assimilation (3D-Var) at a 5-km resolution (detailed in Section 3). The assimilation system requiring fewer computational resources than more advanced systems such as 4D-Var allows to rapidly assimilate the latest observations and to frequently update forecasts.

3 Local Analysis

The analysis cycle (with 5-km gridspacing) combines the 3D-VAR and 1-hour forecasts produced by the numerical model (Figure 1). First, the first guess of 3D-VAR at FT=-3 (3 hours before the initial time) comes from the MSM forecast. After analysis at FT=-3 is conducted by assimilating observations around FT=-3, 1-hour integration from the results is conducted to generate the first guess of the next 3D-VAR at FT=-2. The cycle is repeated, and the final analysis is produced from the last 3D-VAR using the first guess obtained from the 1-hour forecast initialized at FT= -1 and observations around FT= 0 (the initial time).

Currently, observations assimilated in LA come from aircrafts (wind and temperature), wind profilers (wind), ground-based GNSS receivers (precipitable water vapor), Doppler radars (radial velocity), radars (reflectivity), land surface observatory stations (pressure) and radiosondes (wind, temperature, pressure and humidity). In addition, as high resolution enables assimilation for observations locality of which is strong such as temperatures and wind velocity near the surface, the 3D-VAR in the analysis cycle assimilates 1.5-m temperature and 10-m wind velocity data obtained from the automated surface observation network (the nationwide AMeDAS system), while Meso-scale Analysis (MA; the assimilation system used to produce initial conditions for the MSM) does not.

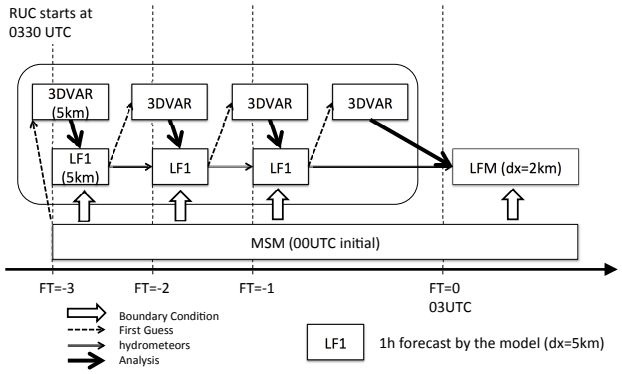

Fig. 1: Schematic diagram of the rapid update cycle (generating analysis at 0300UTC in this case). The cycle repeats assimilation with 3D-VAR and 1-hour forecasts (LF1).

4 Configurations of physical processes in the Local Forecast Model

One of the advantages of higher resolution models is that, needless to say, they can represent smaller scale phenomena. As a result of increasing resolution, parameterizations representing subgrid scale vertical transport can be removed if the grid mean vertical velocity fully represents the vertical transport of momentum, heat and masses including water. In particular, with 2-km horizontal gridspacing, it is considered highly feasible to resolve a significant part of convective transport using the grid mean vertical velocity. In this way, the dependency of physical processes on resolutions comes from partly (or fully) resolved transport, which is parameterized in coarser models. Inhomogeneity within each grid is also a source of the dependency.

Considering the dependency on resolutions, while the LFM and the MSM currently employ the identical non-hydrostatic numerical model package (JMA-NHM), some physical processes employed in the MSM were modified to give higher suitability for the LFM.

For example, no convective parameterizations are adopted in the LFM. As such convective parameterizations could be the origin of significant uncertainty in models, it is preferable not to employ them. Modification has also been introduced to the scheme for diagnosing the width of the probability distribution function (PDF) describing fluctuations of total water amount from grid means, which is used to diagnose cloud fractions. As a result, the width in the LFM can be smaller than that in the MSM because higher resolutions equate to less fluctuation. It has been confirmed that the LFM produces overly large cloud fractions when the PDF width is diagnosed with the same

*E-mail: tabito.hara@met.kishou.go.jp

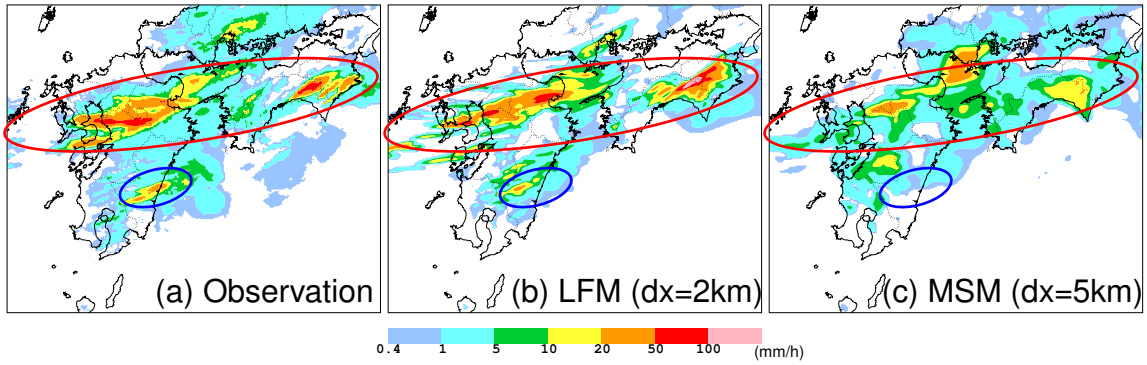

Fig. 2: Examples of forecasts provided by the LFM. All figures show 1-hour accumulated precipitation amounts observed or predicted until 1700UTC on July 11, 2012. (a) Observation, (b) 2-hour forecast by the LFM initialized at 1500UTC on the same day, (c) 5-hour forecast by the MSM initialized at 1200UTC on the same day.

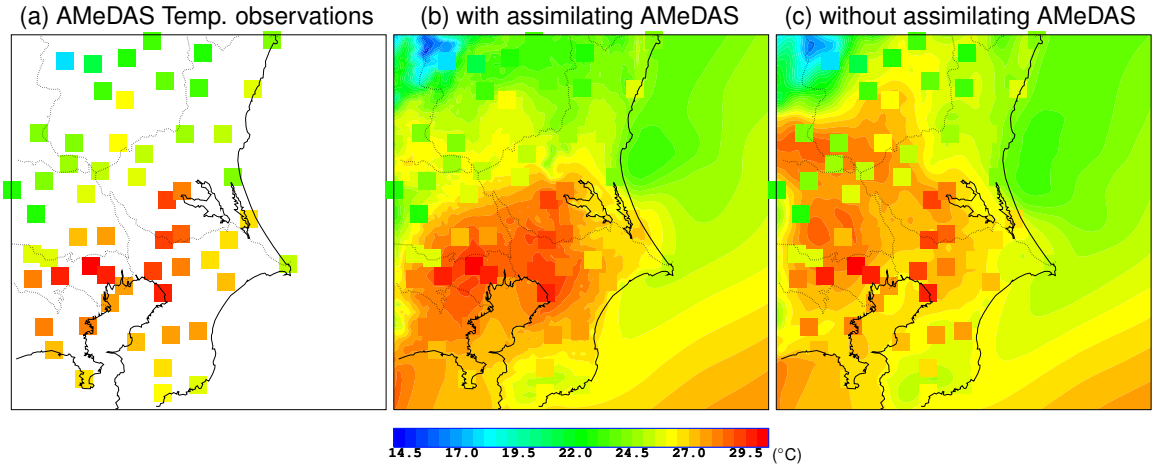

Fig. 3: Examples of analysis to show the effect of assimilating observations near the surface. (a): observation of 1.5-m temperature, (b) and (c) : analysis of 1.5-m temperature (shading) with/without assimilating observations near the surface (obtained from the AMeDAS network) and the corresponding observations (rectangles) with the same color tones as those in the analysis. The results shown in (b) and (c) were produced by the data assimilation systems used in the LFM and the MSM, respectively.

scheme as the MSM, leading to lower daytime surface temperatures and less convection activation.

5 Examples of forecasting and analysis with the Local NWP system

Figure 2 shows the ability of the LFM to accurately predict peak amounts of precipitation contributed by small scale phenomena. In a heavy rainfall event that hit the northern part of Japan's Kyushu Island in July 2012, a stationary front observed around the area over an extended period brought over 500mm of precipitation in a single day. While the MSM predicted the position of the front correctly, the line-shaped precipitation area was not sufficiently generated and the peak value of the predicted precipitation was much lower than the actual amount observed. Meanwhile, the LFM produced the line-shaped precipitation and predicted the peak value of precipitation well, although the positions of the peaks differed slightly from the observed ones. As long as the boundary conditions (i.e. the MSM forecasts in the system), which significantly control synoptic fields in the LFM, give reliable fields, the LFM has considerable potential to reproduce peak values more precisely.

Figure 3 shows the impacts of assimilating observations near the surface. Comparison of the observed temperatures with the analysis field shown in tones of the same color indicates that (b), on which analysis produced by the LA assimilating surface observations are drawn, shows more coincidences between observations and analysis than (c), which indicates analysis generated by the MA without reference to surface observations. More realistic representation in the lower layer can significantly affect forecasting of severe phenomena because temperatures and winds in the lower layer are important in the generation of unstably stratified layers and the initiation of convection.

6 Conclusion

JMA launched a new operational NWP system at a convection-permitting resolution, in which the latest observations are quickly assimilated and forecasts are updated frequently. Some physical processes were modified from those of the coarser operational model in consideration of their dependency on resolutions. As examples, no convective parameterization is employed and the smaller PDF width of the fluctuation of the total water amount is adopted. LFM's potential to predict peak values of precipitation more appropriately was demonstrated.

The current Local NWP system produces forecasts only for the eastern part of Japan and its update frequency is limited to every 3 hours. In 2013, the domain will be expanded to cover the whole of Japan and its surrounding area and hourly operation will begin.

Effect of warm ocean current on the formation of low-level humid air causing a F3 tornado storm observed in middle Japan on 6 May 2012

Teruyuki KATO

Meteorological Research Institute, Tsukuba, Ibaraki, Japan
(E-mail: tkato@mri-jma.go.jp)

1. Introduction

On 6 May, 2012, a strong tornado with Fujita scale 3 (> 70 m/s) struct Tsukuba City, located Kanto Plain in the middle part of Japan (see Fig. 1a). The tornado occurred in a supercell storm that formed mainly due to the northward inflow of low-level humid air from the Pacific Ocean, as well as large temperature difference in the vertical between low and middle levels that maintained from the previous day.

The specific humidity at a height of 500 m became almost doubled from 6 g/kg during 12 hours when the low-level air traveled over the ocean south of the Japanese Islands (Figs. 2a and 2b). This humidified air flowed spotly into Kanto Plain to cause the storm just after 12 JST (= UTC + 9 hours) on 6 May. The increase of specific humidity could be mainly caused by updrafts associated with a low-level short trough travelling eastward (see dashed lines in Figs. 2a and 2b). The value of specific humidity at 06 JST 06 was, however, larger than that near the surface before 12 hours (Fig. 2c). This means that near-surface water vapor increased by latent heat flux from the sea surface, which is ascertained by the increase of about 2 g/kg at 06 JST 06 (Fig. 2d).

Japan Current, a warm ocean current, existed along the route where the near-surface air obtained latent heat flux from the sea surface. In this study, the effect of Japan Current on the formation of low-level humid air is examined using a Japan Meteorological Agency (JMA) nonhydrostatic model with a horizontal resolution of 5 km (Saito et al. 2007).

2. Experimental designs

Eighteen-hour forecasts from 18 JST 05 May 2012 are conducted using initial and boundary conditions produced from 3-hourly available JMA mesoscale analyses with a horizontal resolution of 5 km. Model domain, topography and given sea surface temperature (SST) are shown in Figs. 1a and 1b, and 50 stretched layers (6 of which are set below a height of 500 m) are set in the vertical. A bulk-type microphysics parameterization scheme in which two moments are treated only for ice hydrometeors (i.e., snow, graupel and cloud ice) is used for precipitation processes, and the Kain-Fritsch convection parameterization scheme is additionally used. The turbulence closure scheme is Mellor-Yamada-Nakanishi-Niino level-3 (Nakanishi and Niino 2006). The surface fluxes are calculated by a bulk method, in which the bulk coefficients are determined from the formula of Berjaars and

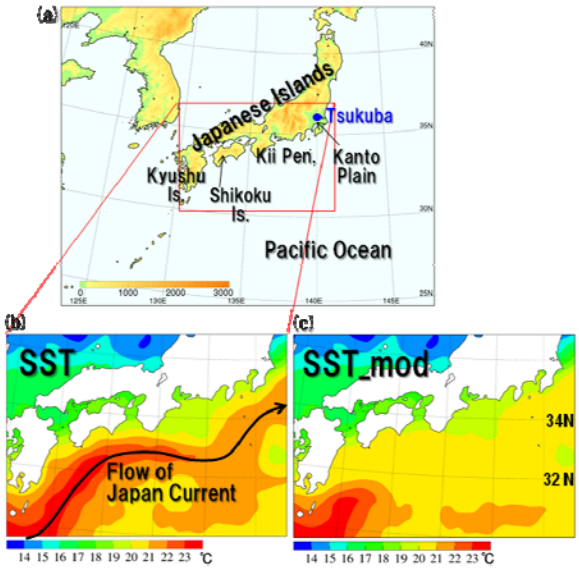

Fig. 1 (a) Model domain and topography of 5km-model and (b) distribution of sea surface temperature on 6 May 2012, depicted from JMA mesoscale analysis. (c) Same as (b), but the maximum sea surface temperature north of 32 °N is set under 20 degrees of Celsius.

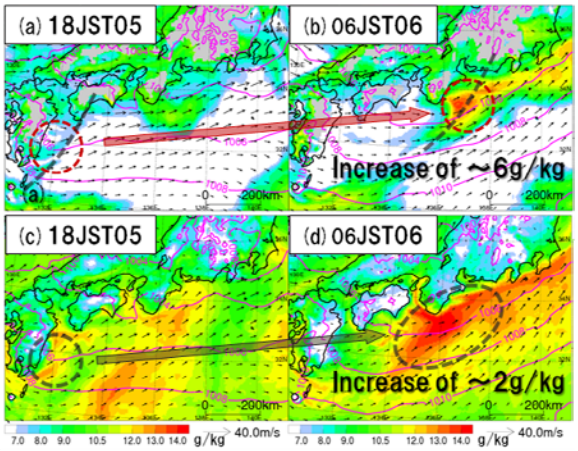

Fig. 2 Horizontal distributions of specific humidity (color), sea level pressure (contour) and horizontal wind vectors at a height of 500m at (a) 18 JST 05 May 2012 and (b) 06 JST 06, depicted from JMA mesoscale analysis. (c) and (d) same as (a) and (c), respectively, but near the surface.

Holtslag (1991) over both sea and land. The other specifications are almost the same as those in Saito et al . (2007).

To examine the effect of Japan Current on the formation of low-level humid air, a sensitivity experiment is also conducted using a modified distribution of SST in which the maximum sea surface temperature north of 32 °N is set under 20 degrees of Celsius (Fig. 1c). This modification eliminates Japan Current located south of the Japan Islands, and lowers the SST up to about 3 degrees (see pink contours in Fig. 4).

3. Results

The forecast accuracy is checked by the distribution of 500m-height specific humidity after 12 hour integration (Fig. 3a). A humid area with a horizontal scale of 100 ~ 200 km is successfully reproduced southeast of Kii Peninsula, although the maximum value is slightly smaller and the low-level short trough slightly travels faster than the analysis (Fig. 2b).

On the other hand, the sensitivity experiment shows that removal of high SST areas associated with Japan Current results into the reduction of low-level water vapor (Fig. 3b). The decrease of 2 g/kg at a height of 500 m corresponds to one-third for the increase of 6 g/kg during 12 hours (Figs. 2a and 2b). Such a decrease of 2 g/kg is also found near the sea surface (not shown). Therefore, additional increase of 2g/kg over Japan Current could be significant to the formation of the storm causing the Tsukuba tornado.

4. Effect of Japan Current on the accumulation processes of low-level water vapor

The effect of Japan Current on the accumulation processes of low-level water vapor with a depth of about 1 km are examined by the differences between the control and sensitivity experiments. Figure 4 shows the differences at 03 JST 6 May 2012, 3 hours later from Fig.3.

It is easy expected that high SST produces warm humid air in the lower layer due to large sensible and latent heat fluxes to induce the pressure drop. This drop is found over Japan Current, and consequently near-surface wind convergence is produced along the Current (Fig. 4a). The convergence intensifies updrafts around the low-level short trough that transports water vapor upward from the near sea surface (Fig. 4b). Noted that such a convergence is not found at a 334-m height. The pressure drop also accelerates near-surface winds (Fig. 4c), which further increases latent heat flux from the sea surface in addition to the increase due to high SST (Fig. 4d). The above-mentioned interaction between air and sea helps the formation of low-level humid air.

References

Beljaars, A.C.M. and A.A.M. Holtslag, 1991: Flux parameterization over land surfaces for atmospheric models. *J. Appl. Meteor.*, **30**, 327-341.

Nakanishi, M. and H. Niino, 2006: An improved Mellor-Yamada level-3 model: Its numerical stability and application to a regional prediction of advection fog. *Bound.-Layer Meteor.*, **119**, 397-407.

Saito, K., J. Ishida, K. Aranami, T. Hara, T. Segawa, M. Nareta, and Y. Honda, 2007: Nonhydrostatic atmospheric models and operational development at JMA. *J. Meteor. Soc. Japan*, **85B**, 271-304.

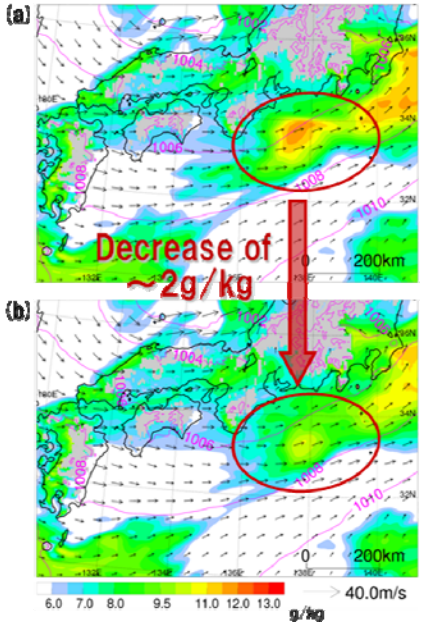

Fig.3 (a) Same as Fig. 2, but 12 hour forecasts of 5km model. (b) Same as (a), but the result of a sensitivity experiment in which SST is given by Fig. 1c.

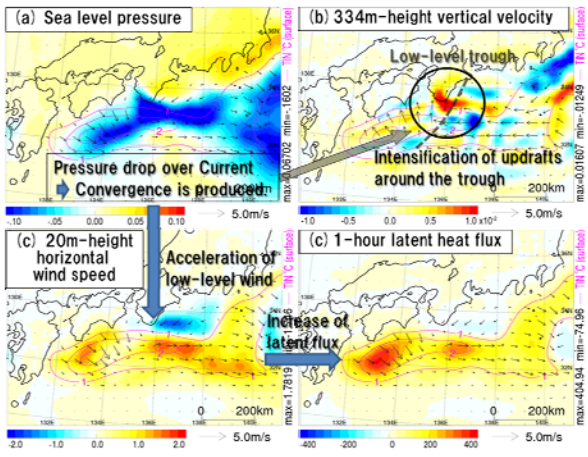

Fig. 4 Horizontal distribution of the differences between control and sensitivity experiments in (a) see level pressure (hPa), (b) 334m-height vertical velocity (m/s), (c) near-surface horizontal wind speed (m/s), and (d) one-hour accumulated latent heat flux (W) at 03 JST 06 May 2012. Pink contours and wind vectors denote the differences in given SST and horizontal winds, respectively.

TRIPLE EYEWALL EXPERIMENT OF THE 2012 TYPHOON "BOLAVEN" USING CLOUD RESOLVING ENSEMBLE FORECAST

Seiji ORIGUCHI[1], Kazuo SAITO[1], Hiromu SEKO[1], Tohru KURODA[2,1] and Wataru MASHIKO[1]
[1]Meteorological Research Institute, Tsukuba, Japan
[2]Japan Agency for Marine Science and Technology, Yokohama, Japan
E-mail; origuchi@mri-jma.go.jp

1. Introduction

Typhoon "BOLAVEN" passed the Okinawa island about 1200 UTC 26th August 2012, while moving northwestward. Compared with the original forecast of JMA, observed surface pressure at the Nago station in the Okinawa island was high, and precipitation and wind speed were weak. The Radar Information Sharing System (RISS) of JMA showed that the typhoon had a clear structure of triple eyewall from 1800 UTC 25th to 0600 UTC 26th. We infer that this multiple eyewall structure might weaken the surface winds and suppressed precipitation insides the eyewalls. In the radar observation, the eyewall replacement wasn't analyzed. On the other hand, JMA's operational mesoscale model (MSM) didn't reproduce the triple eyewall structure of the typhoon. Here, we performed a reproduction experiment with the cloud resolving ensemble forecast to see predictability of the triple eyewall.

2. Methods of experiment

At first, with the initial time at 1200 UTC 25th August, a mesoscale ensemble forecast with a horizontal resolution of 5 km and 11 members was performed up to the forecast time (FT) of 36 hrs using the JMA nonhydrostatic model (JMANHM). Next, its down-scaling (cloud resolving ensemble) forecast with a horizontal resolution of 1 km and 11 members was performed up to FT=24. Control run of the 5km ensemble forecast was conducted using the JMA 4DVAR (JNoVA) mesoscale analysis as the initial condition and the JMA global model (GSM) forecast as the boundary condition. The JMA one-week global ensemble forecast was used as the initial and boundary perturbations. The initial and boundary conditions of the 1 km ensemble forecast is given by the 5km ensemble forecast result with the initial time lag of 6 hrs. Cloud microphysics with the 2-moment 3-ice bulk method and Kain-Fritsch convective parameterization scheme were employed in the 5 km ensemble forecast, while the Kain-Fritsch scheme was switched-off in the 1 km ensemble forecast. A boundary layer model (MYNN3) was used in the 5 km ensemble forecast, while the Deardorff's (1980) TKE scheme was employed in the 1 km ensemble forecast.

3. Reproducible criteria of multiple eyes

Since there are no objective (numerical) evaluation methods about criteria of multiple eyes, we introduce the following criteria:

●Distributions of updrafts or total water substances (Qc+Qr+Qi+Qs+Qg) in the lower troposphere (1 km to 5 km AGL) are ring-shaped structure and continue at least 6 hrs (Even if a part of ring changes spiral or it cuts off for the short time, we ignore it if the ring-shaped structure of updrafts or total water substances keeps overall).

4. Results of experiment and analysis

This section discusses the results of the 1 km ensemble forecast for the period from FT=01 to FT=06. To decide the typhoon's geometric central position precisely, we adopt the Braun's (2002) method, and then we measured the ring shape of multiple eyes for all forecast time. Figure 1 shows results of central position that estimated by the Braun's method and surface

minimum pressure of the model (CNTL and the member M05 only). Though the maximum difference of surface minimum pressures among the ensemble members was about 10hPa, differences between the central pressures decided by the Braun's method and surface minimum pressures for each member were less than 1 hPa (Figure not shown). Next, to analyze the triple eyewall structure, spatial averages of physical elements were calculated on the rings with radius of every 1 km (from 1 km to 600 km) and width 1 km, and temporal averages of physical elements were calculated in 6 hrs between FT=01 and FT=06 (Figure 2). Figure 3(a)(b), (c)(d) and (e)(f) show tangential velocities ([**vt**]st), updrafts ([**w**]st) and liquid water substances ([**Qc+Qr**]st) for CNTL and the member M05 respectively. Radii of the local maximum surface velocity appeared at places about 50 km and 120 km for both CNTL and the member M05, consistent with the observation. However, the inner most eyewall that located on the radius of 10 km wasn't clear in the model (Strong and weak wind shears are shown by black solid lines and broken lines, respectively). Updrafts of middle eyewall were stronger than those of other eyewalls, and the middle eyewall had abundant water substances below 6 km AGL. The regions of strong tangential velocity existed at the outer edges of the eyewalls. Though the outer eyewall wasn't clear compared with the middle eyewall, it had a similar structure. Downdrafts existed between the eyewalls. Although updrafts and liquid water substances in the lower layer appeared at the place of radius 10km, the formation of the inner most eyewall was insufficient in this simulation.

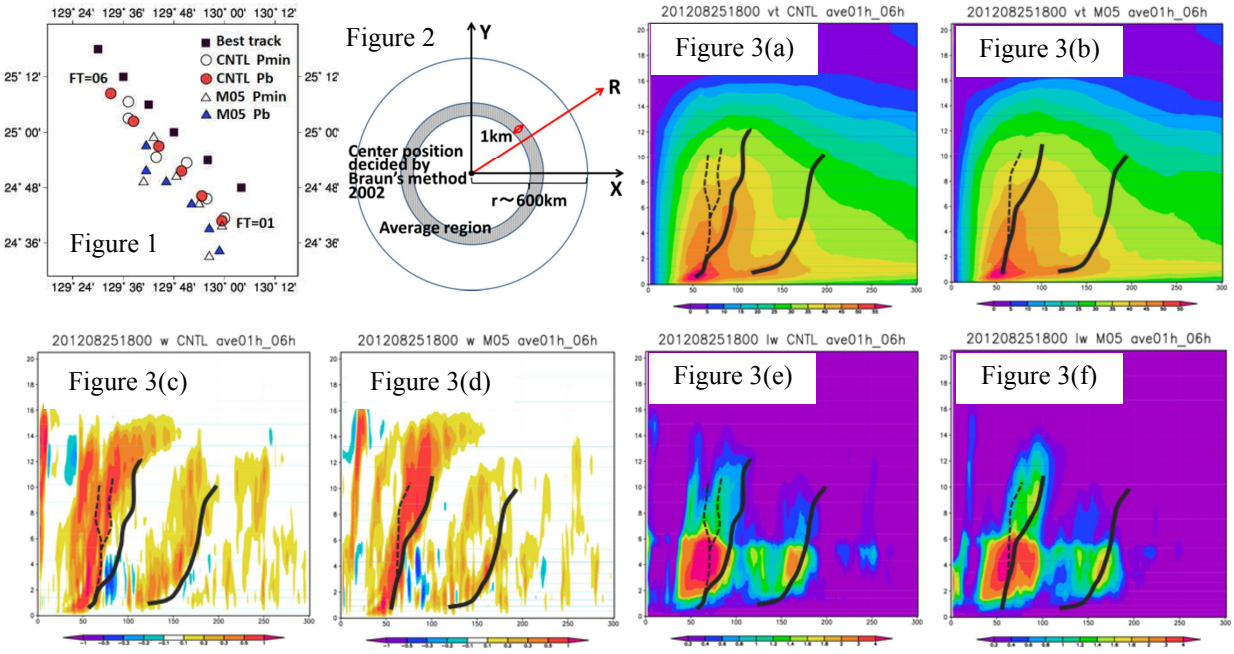

Figure 1: The estimated typhoon's central position by Braun's (2002) method and surface minimum pressure of CNTL and M05.
Figure 2: Calculation method of the averaged physical elements to analyzing the triple eyewall (Spatial average in the shaded region).
Figure 3: The averaged physical elements in 1km ensemble forecast. (a) and (b) show tangential velocities ([**vt**]st) of CNTL and M05 respectively. (c) and (d) show updrafts ([**w**]st) of CNTL and M05 respectively. (e) and (f) show liquid water substances ([**Qc+Qr**]st) of CNTL and M05 respectively.

Reference: Braun, S. A., 2002: A Cloud-Resolving Simulation of Hurricane Bob (1991): Storm Structure and Eyewall Buoyancy. *Mon. Wea. Rev.*, **130**, 1573-1592.
Acknowledgements: Part of the results is obtained by access to the K computer at the RIKEN Advanced Institute for Computational Science. A part of this research has been funded by MEXT Strategic Programs for Innovative Research (SPIRE).